Stability of Water Bells Generated by Jet Impacts on a Disk

C. Clanet
I.R.P.H.E., CNRS–Universités d'Aix-Marseille I & II, Campus Universitaire de St. Jérôme, Service 252, 13397 Marseille Cedex 20, France
(Received 27 March 2000)

Water bells appear when a cylindrical liquid jet impacts normally onto a disk of similar diameter. First observed and described experimentally by F. Savart, their stationary shape was analytically obtained by J. Boussinesq. Here we consider the stability of these bells and derive a general stability criterion showing their sensitivity both to the pressure difference across the liquid sheet and to the ejection angle from the impacting disk. In this later case, we find a critical angle of ejection above which the bell is periodically destroyed and created.

PACS numbers: 47.17.+e, 47.20.–k, 68.10.–m, 68.35.Ja

Historically, the study of liquid sheets was initiated by Savart in 1833 [1–4], following the idea that the precise observation of fluid motion could lead to the understanding of the properties of liquids. These problems are still of interest for practical applications, since the formation of liquid sheets and their stability represent an important element of the atomization process involved, for example, in all engines where the liquid fuel burns as drops. Indeed, industrial observations reveal that the antepenultimate step of the drop production mechanism often consists of the formation and destabilization of liquid sheets. These observations have already initiated several studies [5–7], and initially motivated the present one. From the physical side, the originality of this work does not specifically rest on the description of the stationary shape of the bells but rather on the general stability argument that follows. To our knowledge, the stability of bells has never been considered and the self-oscillating regime never reported.

Prior to the stability, we first consider the problem of the impact of a cylindrical liquid jet of diameter D_0 $[L]$, with the velocity U_0 $[LT^{-1}]$ normally to a disk of diameter D_i $[L]$, under the gravity field g $[LT^{-2}]$. (Terms in brackets indicate the dimension of the parameter: $[L]$ length, $[T]$ time, $[M]$ mass.) The liquid being defined by its density ρ $[ML^{-3}]$, viscosity ν $[L^2T^{-1}]$, and surface tension $\sigma[MT^{-2}]$, for similarity purposes, we characterize the initial fluid state with the nondimensional Reynolds, $\mathrm{Re} \equiv U_0D_0/\nu$, and the Weber, $\mathrm{We} \equiv \rho U_0^2D_0/\sigma$, numbers that, respectively, compare inertia to viscosity and surface tension. (For water, $\rho = 1000$ kg/m^3, $\nu = 10^{-6}$ m^2/s, and $\sigma = 0.073$ kg/s^2.) Depending on the geometrical diameter ratio $X \equiv D_i/D_0$, several scenarios can be expected: In the singular limit $X = 0$, the jet undergoes the classical capillary Savart-Plateau-Rayleigh instability [1,8,9]. The opposite limit $X \gg 1$ leads to the so-called hydraulic jump phenomenon, where a thick and calm layer of fluid is connected to the jet through a thin and rapid layer. The location of the jump critically depends on both the injection parameters and on the limit conditions at infinity [2,10]. In the intermediate domain $X \sim 1$, Savart [2,3] has shown that one can observe symmetrical water bells such as the one presented in Fig. 1.

The experimental setup used to study these bells is presented in Fig. 2. Flowing in a closed loop to maintain its physical characteristics constant (ρ, ν, and σ), the liquid is initially contained in a pressurized reservoir. A flow meter AALBORG enables the accurate control of the jet velocity U_0, defined as the ratio of the flow rate to the exit section area. We use high contraction injectors to achieve a laminar top hat profile jet up to Reynolds numbers of the order of 30 000. The contraction and acceleration of the jet prior to the impact is neglected in the whole paper since the Froude number $\mathrm{Fr} = gh/U_0^2$, based on the distance h from the nozzle to the impactor, never exceeded 10^{-2}. A back light scattering method is used to illuminate the bells, and we observe their stability with a high speed video camera Kodak 4500HS coupled with a personal computer.

Theoretically, we first focus on the stationary shape of water bells, using the notations presented in Fig. 1. Since $X \sim 1$, we neglect the viscous losses on the disk and

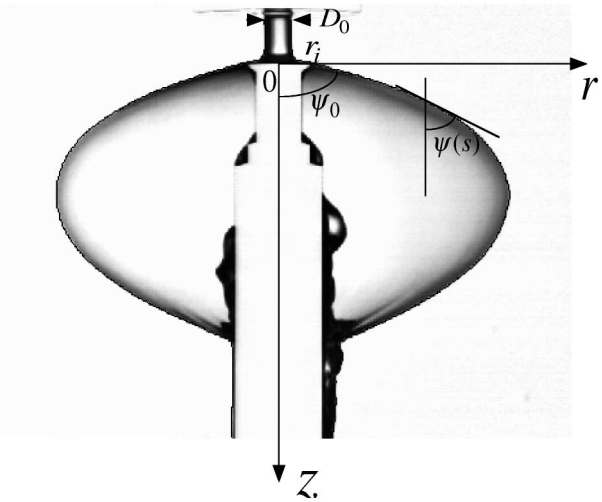

FIG. 1. Water bell obtained with $D_0 = 3$ mm, $U_0 = 2.08$ m/s, and $D_i = 7.33$ mm.

 0031-9007/00/85(24)/5106(4)$15.00

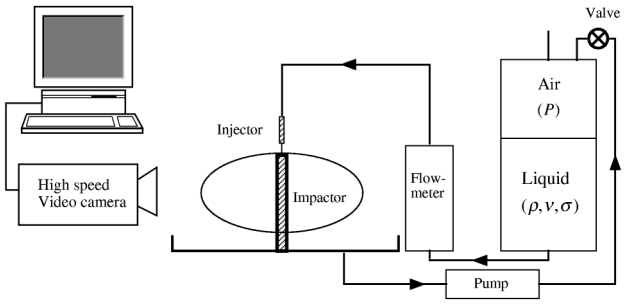

FIG. 2. Experimental setup.

assume that the liquid film is ejected at ($r = r_i = D_i/2$, $z = 0$) with the velocity U_0 and forming the angle ψ_0 with the z axis at the detaching point.

Using U_0 and $l = D_0\mathrm{We}/16$ as the characteristic speed and length, Taylor [11] has shown that the conservation of mass and momentum enable the determination of the bell shape through the integration of the nondimensional system:

$$\tilde{u}^2 = 1 + 2\beta\tilde{z} \tag{1}$$

and

$$(\tilde{u} - \tilde{r})\frac{d\psi}{d\tilde{s}} = -\cos(\psi) + \alpha\tilde{r} - \beta\frac{\sin(\psi)}{\tilde{u}}, \tag{2}$$

where $\alpha \equiv pl/(2\sigma)$ is the reduced pressure difference between the inside and the outside of the bell and $\beta \equiv gl/U_0^2$ is the reduced gravity. All the dimensionless quantities are noticed with a tilde except angles. $\tilde{s}$ stands for the reduced curvilinear location and $\tilde{u}$ for the reduced velocity in the liquid sheet.

Physically, Eq. (1) just expresses the increase of momentum in the direction of the flow due to the acceleration of gravity and Eq. (2) the equilibrium of the liquid sheet in the direction normal to the flow when submitted to centrifugal acceleration, curvature effects, pressure difference, and gravity.

This system of Eqs. (1) and (2) has to be integrated with the initial conditions $\tilde{r}(0) = \tilde{r}_i$ and $(d\tilde{r}/d\tilde{z})_{\tilde{z}=0} = \tan(\psi_0)$.

In the limit $\alpha = 0$ and $\beta \gg 1$, where there is no pressure difference and where the effect of gravity overcomes surface tension, the system (1) and (2) leads to the paraboloid

$$\tilde{z} = \frac{\beta}{2}(\tilde{r} - \tilde{r}_i)^2. \tag{3}$$

In that limit, the fluid particles at the edge of the disk are independent and fall under their own weight.

In the limit $\alpha = 0$ and $\beta \ll 1$, surface tension effects dominate and the integration of the system (1) and (2) leads to the catenary

$$\tilde{r} = 1 - c_1\cosh\left(\frac{\tilde{z} - c_2}{c_1}\right), \tag{4}$$

with the constants of integration

$$c_1 = (1 - \tilde{r}_i)\cos(\psi_0) \quad \text{and} \quad c_2 = c_1\ln\left(\frac{1 + \sin(\psi_0)}{\cos(\psi_0)}\right). \tag{5}$$

This solution was first published 36 years after Savart's work by Boussinesq [12,13]. Compared to the paraboloid, this later shape exhibits a symmetry with regard to the equatorial plane defined by $d\tilde{r}/d\tilde{z} = 0$. This symmetry is broken as soon as gravity starts to play a role. (Looking at horizontal bells, Taylor [11] has shown that air entrainment can also break the symmetry of the bells.)

According to the nondimensional equation (2), the effect of gravity is of the order β compared to the effect of surface tension which implies that the gravitational and the capillary domain are separated by the critical value $\beta \equiv gl/U_0^2 = 1$. Since $l = \mathrm{We}/16D_0$, β reduces to $\beta = (D_0/a)^2/8$, where $a \equiv \sqrt{2\sigma/(\rho g)}$ is the capillary length of the liquid-air interface (for water on earth, $a \approx 3.8$ mm). In our applications, β never exceeded 0.1 and the shapes (Fig. 1) clearly exhibit a symmetry with regard to the equatorial plane. Moreover, the condition $\alpha = 0$ was experimentally achieved using a straw connecting both sides of the bell. These conditions justify the comparison of the Boussinesq's solution to the experimental shapes obtained with an edge detection algorithm presented as a black continuous line in Fig. 1. If ψ_0 is given, this solution compares well with the shape extracted from the pictures as presented in Fig. 3.

Considering the stability of the closed capillary bells, two different examples of unstable sheets are presented in Figs. 4 and 5. In Fig. 4, we start the experiment with a stable bell (top left image) similar to the one presented in Fig. 1, and we progressively decrease the flow rate. This induces a pressure increase which triggers at one point a

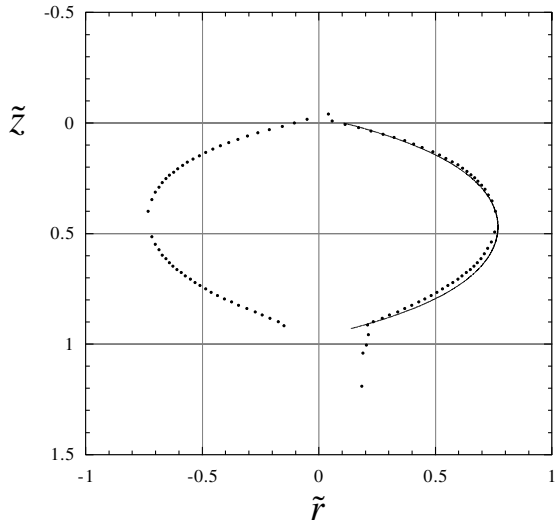

FIG. 3. Comparison between the Boussinesq catenary solution and the water bell shape extracted from Fig. 2.

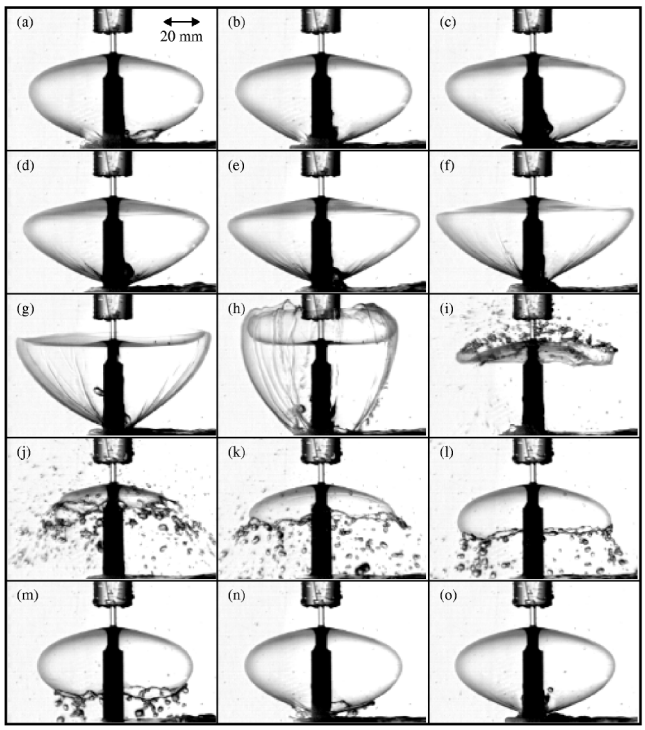

FIG. 4. Instability triggered by a pressure decrease, observed with $\psi_0 = 77°$, $D_0 = 3.0$ mm, $D_i = 9.87$ mm, and $U_0 = 2.7$ m/s. Time increases from left to right and from top to bottom with the time step $\Delta t = 35.5$ ms.

shape transformation and the bursting of the bell. The triggering mechanism is thus removed at the bursting since the pressures are equalized, and if we stop decreasing the flow rate at the beginning of the transformation, the daughter bell (bottom right image) remains stable. If we continue to decrease the velocity, the bell will undergo a similar transformation and we can get up to 10 generations of bells, each of them being smaller than the previous one and larger than the following one.

The phenomenon presented in Fig. 5 is very different in the sense that the cycle presented reproduces itself periodically without any change of the flow rate or other control parameter. The only difference with the stable bell presented in Fig. 1 is the ejection angle which is here closer to $\pi/2$. That cycle also leads from a mother bell to a daughter bell, identical to the mother and that will, once closed, undergo the same unstable scenario without any change of the initial conditions. In that particular case, bells are created and destroyed with a frequency close to 2 Hz.

The main observation on the bells stability concerns the influence of the pressure difference, p. If that difference is kept equal to zero, the resulting bells always remain stable. The origin of the bells' stability thus lies in the pressure difference effect, or more precisely in the reaction of the bell to a pressure difference perturbation. Let us first imagine that following a pressure increase inside the bell, the volume of the whole bell increases. In that case, the reaction of the bell tends to compensate the origin of the perturbation and one expects the bell to remain stable. On the contrary, if the bell volume decreases following a pressure increase, the bell reaction amplifies the perturbation and one may expect, at the end, the full bursting of the

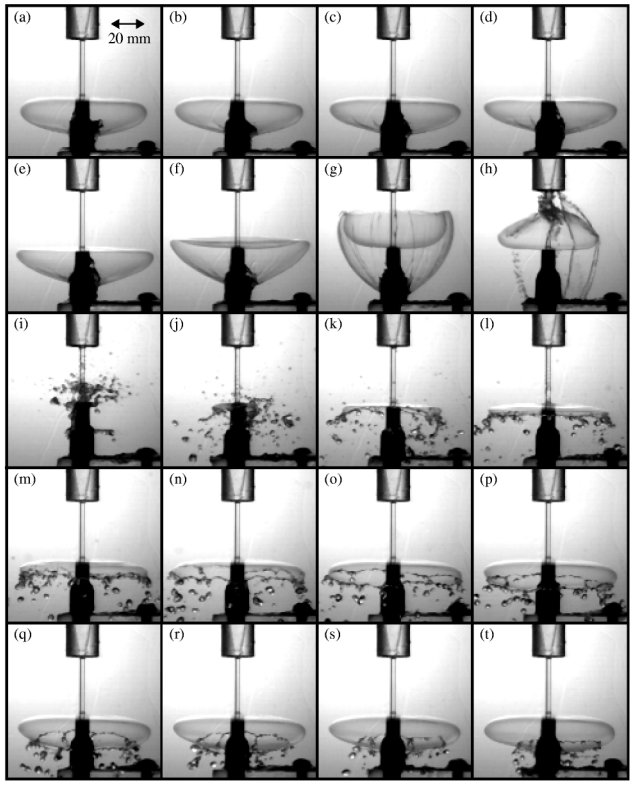

FIG. 5. Instability characterized by a large angle of ejection $\psi_0 = 87°$, observed with $D_0 = 3.0$ mm, $D_i = 10.0$ mm, and $U_0 = 2.21$ m/s. Time increases from left to right and from top to bottom with the time step $\Delta t = 27.7$ ms.

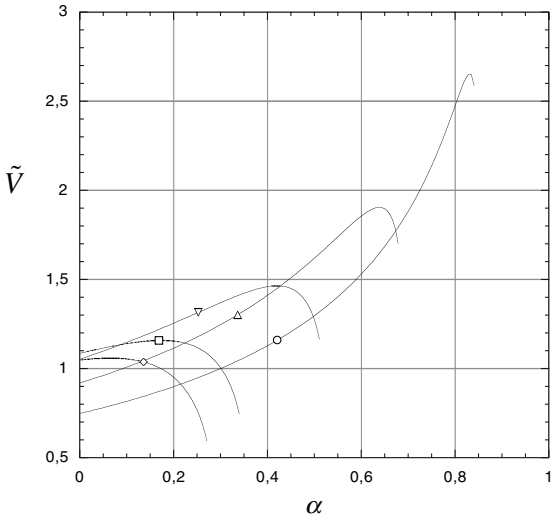

FIG. 6. Evolution of the nondimensional volume $\tilde{V}$ with the pressure α, for different values of ψ_0: ○, 65°; △, 70°; ▽, 75°; □, 80°; ◇, 85°.

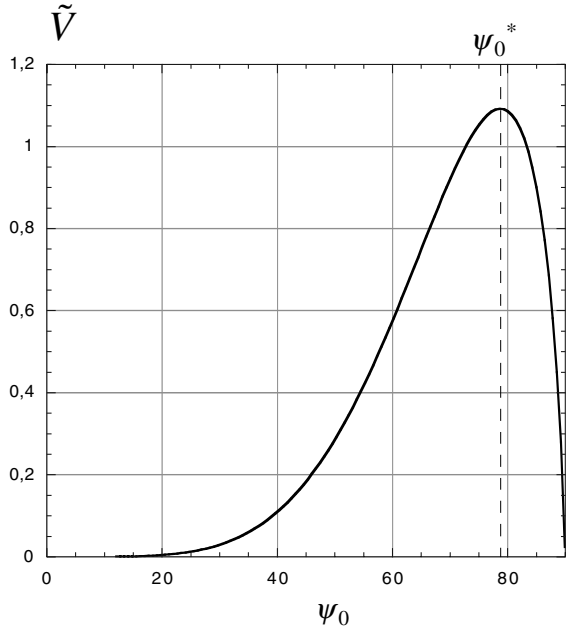

FIG. 7. Evolution of the nondimensional volume $\tilde{V}$ with the ejection angle ψ_0.

bell. This analysis leads to the stability criterion,

$$\frac{dV}{dp} \geq 0\,, \tag{6}$$

where V is the volume of the closed bell. Looking at the system (1) and (2) in the limit $\beta \ll 1$, we get that $V \equiv l^3\pi \int_0^{\tilde{z}_{\max}} \tilde{r}^2\, d\tilde{z}$ defined using the maximal location on z, $\tilde{z}_{\max}$, is a function of three parameters $V(l, \alpha, \psi_0)$. Noticing that l and p are independent, the stability criterion (6) can be written as

$$\frac{d\tilde{V}}{dp} = \frac{1}{l^3}\frac{dV}{dp} = \left(\frac{\partial \tilde{V}}{\partial \alpha}\right)_{\psi_0} \frac{l}{2\sigma} + \left(\frac{\partial \tilde{V}}{\partial \psi_0}\right)_{\alpha} \frac{d\psi_0}{dp}\,. \tag{7}$$

We first concentrate on the case where the first term in the right-hand side of Eq. (7) dominates, that is, where ψ_0 almost remains constant and where the driving mechanism is the pressure difference α. For different ejection angles ψ_0, the evolution $\tilde{V}(\alpha)$, obtained through the numerical integration of the system (1) and (2), is presented in Fig. 6. These curves all exhibit a maximum, the value of which increases when the angle ψ_0 is decreased. According to Eq. (7), one deduces that the corresponding bells are stable for the small values of α and become unstable once the maximum is passed. Since the bursting of the bell leads to $\alpha = 0$, one expects the instability to occur once. This limit corresponds to the instability presented in Fig. 4.

We now concentrate on the limit where the second term in Eq. (7) dominates, that is, around $\alpha = 0$, where according to Fig. 6 $(\partial \tilde{V}/\partial \alpha)_{\psi_0} = 0$. Making the statement that

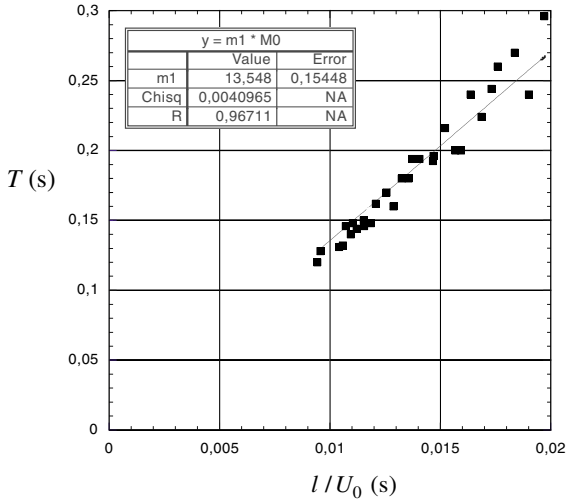

FIG. 8. Evolution of the self-sustained oscillation period T, with the characteristic time of regeneration l/U_0.

ψ_0 results from the local balance of forces at the point of detachment, one deduces that $d\psi_0/dp > 0$ and the stability of the bell depends only on the sign of $(\partial \tilde{V}/\partial \psi_0)_{\alpha=0}$. For $\alpha = 0$, we use the catenary of Boussinesq to evaluate $\tilde{V}(\psi_0)$. This evolution is presented in Fig. 7 and clearly exhibits a maximum value at $\psi_0^\star = 78.8°$. That value separates the stable bells $(\psi_0 < \psi_0^\star)$ where $(\partial \tilde{V}/\partial \psi_0)_{\alpha=0} > 0$ from the unstable ones $(\psi_0 > \psi_0^\star)$ where $(\partial \tilde{V}/\partial \psi_0)_{\alpha=0} < 0$.

In this later case, the instability also leads to the bursting of the bell which keeps $\alpha = 0$ but does not affect the origin of the instability, $\psi_0 > \psi_0^\star$. One thus expects the instability to reproduce itself continuously. This limit corresponds to the instability presented in Fig. 5. The period T of the instability is presented in Fig. 8 as a function of the regeneration time l/U_0. This figure suggests a linear relationship $T \approx 13.5 l/U_0$.

[1] F. Savart, Ann. De Chim. **53**, 337–386 (1833).
[2] F. Savart, Ann. De Chim. **54**, 56–87 (1833).
[3] F. Savart, Ann. De Chim. **54**, 113–145 (1833).
[4] F. Savart, Ann. De Chim. **55**, 257–310 (1833).
[5] N. Dombrowski and R. P. Fraser, Philos. Trans. A **247**, 101–130 (1954).
[6] G. I. Taylor, Proc. R. Soc. London A **253**, 313–321 (1959).
[7] F. H. Bark, H.-P. Wallin, M. G. Gallstedt, and L. P. Kristiansson, J. Fluid Mech. **90**, 625–639 (1979).
[8] J. Plateau, *Statique Expérimentale et Théorique des Liquides* (Gauthier-Villars et Cie., Paris, 1873).
[9] Lord Rayleigh, Proc. London Math. Soc. **10**, 4–13 (1879).
[10] E. J. Watson, J. Fluid Mech. **20**, 481–499 (1964).
[11] G. I. Taylor, Proc. R. Soc. London A **253**, 289–295 (1959).
[12] J. Boussinesq, C.R. Acad. Sci. Paris **69**, 45–48 (1869).
[13] J. Boussinesq, C.R. Acad. Sci. Paris **69**, 128–131 (1869).